Article:
Hunter, S.J. orcid.org/0000-0002-9280-1969, Penfold, N.J.W., Chan, D.H. et al. (2 more authors) (2020) How do charged end-groups on the steric stabilizer block influence the formation and long-term stability of Pickering nanoemulsions prepared using sterically stabilized diblock copolymer nanoparticles? Langmuir, 36 (3). pp. 769-780. ISSN 0743-7463

https://doi.org/10.1021/acs.langmuir.9b03389

How do Charged End-Groups on the Steric Stabilizer Block Influence the Formation and Long-Term Stability of Pickering Nanoemulsions Prepared using Sterically-stabilized Diblock Copolymer Nanoparticles?

Saul J. Hunter, Nicholas J. W. Penfold, Derek H. Chan,
Oleksandr O. Mykhaylyk and Steven P. Armes*

[†]Department of Chemistry, Dainton Building, University of Sheffield,
Brook Hill, Sheffield, Yorkshire S3 7HF, UK.

* Author to whom correspondence should be addressed
(s.p.armes@sheffield.ac.uk)

ABSTRACT. Reversible addition-fragmentation chain transfer (RAFT) solution polymerization is used to prepare well-defined poly(glycerol monomethacrylate) (PGMA) chains bearing either carboxylic acid, tertiary amine or neutral end-groups. Each of these PGMA precursors was then chain-extended in turn via RAFT aqueous emulsion polymerization of 2,2,2-trifluoroethyl methacrylate (TFEMA) to form spherical nanoparticles as confirmed by TEM analysis. DLS studies indicated an intensity-average diameter of approximately 25 nm. Aqueous electrophoresis measurements confirmed that the amine-functional nanoparticles became cationic at low pH owing to end-group protonation. In contrast, carboxylic acid-functional nanoparticles became appreciably anionic at pH 10 owing to end-group ionization. Finally, nanoparticles bearing neutral end-groups exhibited zeta potentials of close to zero over a range of solution pH. High-shear homogenization of *n*-dodecane in the presence of such sterically-stabilized nanoparticles led to the formation of oil-in-water Pickering *macroemulsions* with volume-average diameters of 20 to 30 μm. High-pressure microfluidization was then used to prepare the three corresponding Pickering *nanoemulsions*. Each Pickering nanoemulsion was characterized by analytical centrifugation and TEM studies of the dried nanoemulsion droplets confirmed their original nanoparticle superstructure. The nanoparticle adsorption efficiency at the oil-water interface was assessed by gel permeation chromatography (using a UV detector) for each nanoparticle type at both pH 3 and 7. Nanoparticles with charged end-groups exhibited relatively low adsorption efficiency, whereas up to 90% of the neutral nanoparticles were adsorbed onto the oil droplets. This observation was supported by small-angle X-ray scattering (SAXS) experiments, which indicated that the packing efficiency of neutral nanoparticles around oil droplets was higher than that of nanoparticles bearing charged end-groups. Analytical centrifugation was used to evaluate the colloidal stability of the aged Pickering nanoemulsions. Pickering nanoemulsions stabilized with nanoparticles bearing charged end-groups proved to be significantly less stable than those prepared using neutral end-groups.

INTRODUCTION

As independently recognized by Pickering and Ramsden more than a century ago, Pickering emulsions comprise either oil or water droplets stabilized by solid particles.[1-2] Common Pickering emulsifiers include inorganic particles such as silica,[3-4] titania[5] or clay platelets.[6] However, droplets can also be stabilized by organic particles, such as cellulose-based rods[7-8] or polymer latexes.[9-10] Pickering macroemulsions are widely reported in the literature, with examples including oil-in-water (o/w),[11-12] water-in-oil (w/o),[13-14] and, more recently, water-in-water (w/w)[15-17] and oil-in-oil (o/o).[18] The emulsion type is primarily determined by the particle wettability at the oil-water interface, although the relative volume fraction of the oil phase can also play a role.[11, 19-21]

In recent years, there has been growing interest in Pickering *nanoemulsions*, which comprise droplets of less than approximately 200 nm in diameter.[22-30] In contrast to conventional macroemulsions, nanoemulsions are much less prone to gravitational creaming or sedimentation.[31-32] Furthermore, their significantly higher surface area confers greater activity when used in various cosmetics,[33] drug delivery,[34-35] food[29, 36-37] and agrochemical formulations.[31, 38-40] However, many nanoemulsions suffer from Ostwald ripening.[24-25, 27, 40-41] In principle, this instability mechanism can be suppressed by selecting a highly water-insoluble oil (or by adding such an oil to the nanoemulsion formulation).[24, 27]

The recent development of polymerization-induced self-assembly (PISA) has enabled the convenient synthesis of well-defined diblock copolymer nanoparticles.[12, 42-45] This powerful and versatile technique allows the convenient synthesis of 20-25 nm spherical nanoparticles in the form of a concentrated dispersion by, for example, reversible addition-fragmentation chain transfer (RAFT) aqueous emulsion polymerization.[12, 45-54] The resulting sterically-stabilized nanoparticles can be used to prepare either Pickering macroemulsions[12, 55] or

Pickering nanoemulsions.[25, 27] RAFT polymerization also provides convenient access to a wide range of functional end-groups, which can be readily controlled by using a specific chain transfer agent (CTA).[56-58] In PISA formulations, such end-groups are located at the terminus of the steric stabilizer chains of the block copolymer nanoparticles. Thus they can directly influence the nanoparticle surface charge and can also be used to induce changes in copolymer morphology or colloidal stability.[59-63]

Thompson *et al.*[25] recently reported that 25 nm diameter diblock copolymer nanoparticles can be used in combination with high-pressure microfluidization to produce oil-in-water Pickering nanoemulsions. Subsequently, the effect of varying the aqueous solubility of the *n*-alkane droplet phase on the long-term stability of the nanoemulsions was examined.[27] Analytical centrifugation was used to assess droplet coarsening over time. Pickering nanoemulsions prepared using either *n*-octane or *n*-decane proved to be significantly less stable towards Ostwald ripening than those prepared with either *n*-dodecane or *n*-tetradecane. This difference was rationalized in terms of the greater aqueous solubility of the pair of lower *n*-alkanes. Furthermore, the nanoemulsion composed of *n*-dodecane droplets displayed superior long-term stability compared to a silica-stabilized Pickering nanoemulsion prepared using the same oil reported by Persson *et al.*[24] This marked difference was attributed to the much greater interfacial stress exhibited by sterically-stabilized soft spheres compared to 'hard sphere' silica particles, as reported by Vermant and co-workers.[64]

Preparing stable Pickering emulsions using charged nanoparticles can be rather problematic[3, 65-69] owing to strong repulsive electrostatic interactions between particles. This can offset the particle detachment energy to such an extent that the overall energy of adsorption is comparable to the thermal energy of the nanoparticles. Furthermore, the oil-water interface is known to possess anionic character,[70-71] which may hinder the adsorption of nanoparticles with the same surface charge.[72-73] In order to utilize highly-charged

nanoparticles as efficient emulsifiers, additives such as oppositely-charged surfactants are sometimes employed that adsorb onto the nanoparticles and hence reduce their effective surface charge.[3, 6, 72-73]

The aim of the current study is to examine the effect of systematically varying the surface charge of model sterically-stabilized diblock copolymer nanoparticles (see Figure 1) on their emulsifier performance during the production of Pickering nanoemulsions via high-pressure microfluidization. In addition, the effect of surface charge on the long-term stability of such Pickering nanoemulsions is assessed using analytical centrifugation.

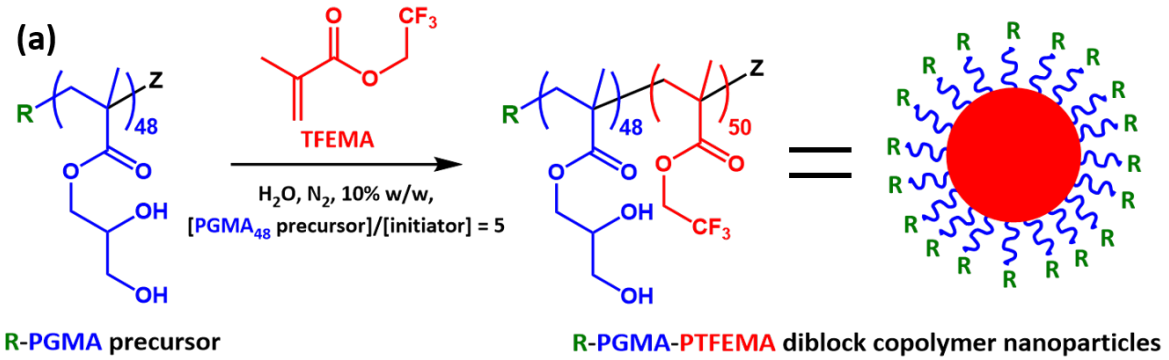

(b)

CTA	R group	Z-group	Reaction conditions
CPDB		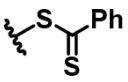	ACVA initiator, 70 °C, pH 6
PETTC	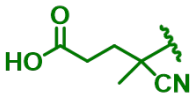	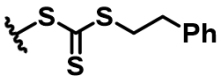	ACVA initiator, 70 °C, pH 3
MPETTC	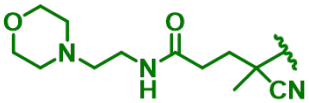	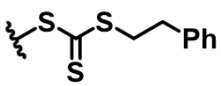	VA-044 initiator, 44 °C, pH 7

Figure 1. (a) Synthesis of $PGMA_{48}$-$PTFEMA_{50}$ diblock copolymer nanoparticles via RAFT aqueous emulsion polymerization of TFEMA, using CPDB, PETTC, or MPETTC RAFT agents, which confer either neutral (0), anionic (-) or cationic (+) end-groups on the $PGMA_{48}$ steric stabilizer chains at a solution pH of 6, 7 or 3, respectively. (b) Summary of the chemical structures for the diblock copolymers synthesized using either CPDB, PETTC or MPETTC and the specific reaction conditions used in each case.

EXPERIMENTAL

Materials. All reagents were used as received unless otherwise stated. Glycerol monomethacrylate (99.8% purity) was obtained from GEO Specialty Chemicals (Hythe, UK). 2-Cyano-2-propyl benzodithioate, 2,2,2-trifluoroethyl methacrylate (TFEMA), 4,4'-azobis(4-cyanopentanoic acid) (ACVA), *n*-dodecane, and deuterium oxide were purchased from Aldrich (UK). 2-Cyano-2-propyl dithiobenzoate (CPDB) was purchased from STREM Chemicals Ltd. (Cambridge, UK). The 4-cyano-4-(2-phenylethanesulfanylthiocarbonyl)sulfanylpentanoic acid (PETTC) RAFT agent was synthesized as previously reported.[43] The morpholine-PETTC (MPETTC) RAFT agent was also synthesized as previously reported.[61] d_6-Acetone and d_4- methanol were purchased from Goss Scientific Instruments Ltd. (Cheshire, UK). All other solvents were purchased from Fisher Scientific (Loughborough, UK). Deionized water was used for all experiments.

Synthesis of $PGMA_{48}$ Macro-CTA via RAFT Solution Polymerization in Ethanol. Three $PGMA_{48}$ macro-CTAs were synthesized via RAFT polymerization of glycerol monomethacrylate in ethanol at 70 °C, using either neutral CPDB, carboxylic acid-functional PETTC or morpholine-functional MPETTC as the RAFT agent to produce (0) $PGMA_{48}$, (-) $PGMA_{48}$ or (+) $PGMA_{48}$ (see Figure 1), as described previously.[12, 59, 61] ^{1}H NMR studies indicated a mean DP of 48 via end-group analysis in each case (integrated aromatic RAFT end-group signals at 7.1−7.4 ppm were compared to those of the two oxymethylene protons at 3.5−4.4 ppm).

Synthesis of $PGMA_{48}$−$PTFEMA_{50}$ Diblock Copolymer Nanoparticles via RAFT Aqueous Emulsion Polymerization of TFEMA

A typical protocol for the synthesis of neutral (0) $PGMA_{48}$-$PTFEMA_{50}$ diblock copolymer nanoparticles was conducted as follows. (0) $PGMA_{48}$ (0.398 g, 0.050 mmol), TFEMA

monomer (0.420 g, 2.5 mmol and ACVA (2.79 mg, 0.010 mmol; $PGMA_{48}$ macro-CTA/ACVA molar ratio = 5.0) and deionized water (7.37 g, 10% w/w) were added to a 14 mL reaction vessel. This aqueous reaction solution was deoxygenated using nitrogen gas for 30 min at 20 °C prior to immersion into an oil bath set at 70 °C. After 6 h, the TFEMA polymerization was quenched by exposing the reaction mixture to air and cooling to ambient temperature.

A typical protocol for the synthesis of anionic (-) $PGMA_{48}$-$PTFEMA_{50}$ diblock copolymer nanoparticles was conducted as follows. (-) $PGMA_{48}$ (0.401 g, 0.050 mmol), TFEMA monomer (0.415 g, 2.5 mmol and ACVA (2.80 mg, 0.01 mmol; $PGMA_{48}$ macro-CTA/ACVA molar ratio = 5.0) and deionized water (7.41 g, 10% w/w) were added to a 14 mL reaction vessel. The pH was adjusted to pH 3 using 1 M HCl. This reaction solution was deoxygenated using nitrogen gas for 30 min at 20 °C prior to immersion into an oil bath set at 70 °C. After 6 h, the TFEMA polymerization was quenched by exposing the reaction mixture to air and cooling to ambient temperature.

A typical protocol for the synthesis of cationic (+) $PGMA_{48}$-$PTFEMA_{50}$ diblock copolymer was conducted as follows. (+) $PGMA_{48}$ (0.402 g, 0.05 mmol), TFEMA monomer (0.415 g, 2.5 mmol and VA-044 (3.19 mg, 0.01 mmol; $PGMA_{48}$ macro-CTA/VA-044 molar ratio = 5.0) and deionized water (7.38 g, 10% w/w) were added to a 14 mL reaction vessel. The pH was adjusted to pH 7 using 1 M NaOH. This reaction solution was deoxygenated using nitrogen gas for 30 min at 20 °C prior to immersion into an oil bath set at 44 °C. After 6 h, the TFEMA polymerization was quenched by exposing the reaction mixture to air and cooling to ambient temperature.

Preparation of $PGMA_{48}$-$PTFEMA_{50}$-Stabilized Pickering Macroemulsions Using High-Shear Homogenization. An aqueous dispersion of $PGMA_{48}$-$PTFEMA_{50}$ nanoparticles (4.0 mL, 7.0% w/w) was added to a 14 mL glass vial. The pH was adjusted to either pH 7 or pH 3

using 1 M NaOH or HCl respectively and then homogenized with *n*-dodecane (1.0 mL) for 2.0 min at 20 °C using an IKA Ultra-Turrax T-18 homogenizer equipped with a 10 mm dispersing tool and operating at 13 500 rpm.

Preparation of $PGMA_{48}$-$PTFEMA_{50}$-Stabilized Pickering Nanoemulsions Using High-Pressure Microfluidization. A Pickering macroemulsion (5.0 mL, initial nanoparticle concentration in the aqueous phase = 7.0% w/w) was further processed using an LV1 low-volume microfluidizer processor (Microfluidics, USA). The pressure was fixed at 20 000 psi and each emulsion was passed ten times through the LV1 unit to achieve well-defined Pickering nanoemulsions.

^{1}H NMR Spectroscopy. All ^{1}H NMR spectra were recorded at 400 MHz in d_6-acetone or d_4-methanol using a Bruker Avance-400 spectrometer with 64 scans being averaged per spectrum.

Gel Permeation Chromatography (GPC). 0.50% w/w copolymer solutions were prepared in HPLC-grade DMF containing 10 mM LiBr and DMSO (1.0 % v/v) was used as a flow-rate marker. GPC studies were conducted at 60 °C using a constant flow rate of 1.0 mL min^{-1}. The GPC set-up comprised an Agilent 1260 Infinity series degasser and pump, an Agilent PL-gel guard column, two Agilent PL-gel 5 μm Mixed-C columns and a refractive index detector. Sixteen near-monodisperse poly(methyl methacrylate) standards ranging from M_p = 645 to 2 480 000 g mol^{-1} were used for calibration.

Dynamic Light Scattering (DLS). Intensity-average hydrodynamic diameters were obtained by DLS using a Malvern Zetasizer NanoZS instrument at a fixed scattering angle of 173°. Aqueous dispersions of 0.1% w/w nanoemulsions were analyzed using disposable cuvettes, and the results were averaged over three consecutive runs, each comprising ten analyses. The deionized water used to dilute each sample was ultrafiltered through a 0.20 μm membrane in order to remove extraneous dust.

Aqueous Electrophoresis. Aqueous electrophoresis studies were performed on 0.10% w/w aqueous copolymer dispersions containing 1 mM KCl as background electrolyte using a Malvern Zetasizer NanoZS instrument at 25 °C. The pH of the copolymer dispersion was initially weakly basic and lowered using HCl. Zeta potentials were calculated from the Henry equation using the Smoluchowski approximation. All data were averaged over three consecutive runs.

Transmission Electron Microscopy (TEM). Nanoemulsion dispersions were diluted fifty-fold using deionised water at either pH 3 or 7 at 20 °C to produce 0.20% w/w dispersions for transmission electron microscopy (TEM) studies. Copper/palladium TEM grids (Agar Scientific, UK) were surface-coated in-house to produce a thin film of amorphous carbon. The grids were then plasma glow-discharged for 30 s to create a hydrophilic surface. Individual samples (0.20% w/w, 10 μL) were adsorbed onto the freshly-treated grids for 1 min and then blotted with filter paper to remove excess solution. To stain the copolymer aggregates, uranyl formate solution (0.75% w/w, 9 μL) was soaked on the sample-loaded grid for 20 s and then carefully blotted to remove excess stain. Each grid was then carefully dried using a vacuum hose. Imaging was performed using a FEI Tecnai Spirit microscope fitted with a Gatan 1kMS600CW CCD camera operating at 80 kV.

Analytical Centrifugation (LUMiSizer). Droplet size distributions were assessed using a LUMiSizer analytical photocentrifuge (LUM GmbH, Berlin, Germany) at 20 °C. Measurements were conducted on diluted Pickering nanoemulsions (1.0% v/v *n*-dodecane) in 2 mm path length polyamide cells at 400 rpm for 200 profiles (allowing 10 s between profiles) and then the rate of centrifugation was increased up to 4000 rpm for a further 800 profiles. The slow initial rate of centrifugation enabled detection of any larger oil droplets that might be present within the nanoemulsion. The LUMiSizer instrument employs space- and time-resolved extinction profiles (STEP) technology to measure the intensity of

transmitted near-infrared light as a function of time and position over the entire cell length simultaneously. The gradual progression of these transmission profiles contains information on the rate of creaming of the oil droplets and hence enables assessment of the droplet size distribution.

Small-Angle X-Ray Scattering (SAXS)

SAXS data were recorded using a laboratory SAXS beamline (Xeuss 2.0, Xenocs, France) equipped with a liquid gallium MetalJet X-ray source (Excillum, Sweden) (wavelength λ = 0.134 nm), two sets of motorized scatterless slits for beam collimation and a Pilatus 1M two-dimensional pixel SAXS detector (Dectris, Switzerland) (sample-to-detector distance = 1.889 m). A flow-through glass capillary (2 mm diameter) was connected to an injecting syringe and a waste container via plastic tubing and mounted horizontally on the beamline stage; this set-up was used as a sample holder. SAXS patterns were recorded using an exposure time of 600 seconds over a q range of 0.02 nm^{-1} to 1.4 nm^{-1}, where $q = (4\pi\sin\theta)/\lambda$ is the length of the scattering vector and θ is one-half of the scattering angle. Data were reduced, calibrated and integrated using the Foxtrot software package supplied with the instrument and further analyzed (background subtraction and data modeling) using Irena SAS macros[74] for Igor Pro.

RESULTS AND DISCUSSION

The $PGMA_{48}$-$PTFEMA_{50}$ nanoparticles used in this study were prepared by RAFT aqueous emulsion polymerization of TFEMA at 10% w/w solids using three different $PGMA_{48}$ precursors in turn (see Figure 1). These precursors were prepared using either neutral CPDB, carboxylic acid-functional PETTC or morpholine-functional MPETTC as the RAFT agent to confer either neutral, anionic or cationic end-groups, as shown in Figure 1a. In each case, the aqueous solution pH was adjusted prior to polymerization to ensure that each RAFT end-group remained in its neutral form. An amidine-based azo initiator (VA-044)

was used for the synthesis of the (+) $PGMA_{48}$ precursor, whereas a carboxylic acid-based azo initiator (ACVA) was employed for the synthesis of the (-) $PGMA_{48}$ precursor.

All three TFEMA polymerizations proceeded to high conversion within 6 h as judged by both ^{1}H and ^{19}F NMR spectroscopy (see Figure S1). The latter technique is particularly convenient because ^{19}F has 100% abundance and ^{19}F NMR spectra do not require deuterated solvents. Moreover, unlike ^{1}H NMR spectra, ^{19}F NMR spectra typically do not suffer from overlapping signals. For (0) $PGMA_{48}$-$PTFEMA_{50}$ and (+) $PGMA_{48}$-$PTFEMA_{50}$ nanoparticles DMF GPC analysis indicated an identical M_n of 23 600 g mol^{-1} and relatively low M_w/M_n values of 1.12 and 1.16, respectively (see Figure S2). The same technique indicated an M_n of 29 700 g mol^{-1} and an M_w/M_n of 1.25 for (-) $PGMA_{48}$-$PTFEMA_{50}$ nanoparticles. The higher M_n value is the result of a high molecular weight shoulder (see the corresponding GPC trace shown in Figure S2). Nevertheless, these amphiphilic diblock copolymer chains form well-defined sterically-stabilized nanoparticles of comparable mean particle diameter (see below).

Transmission electron microscopy (TEM) images confirmed that well-defined spherical nanoparticles were obtained regardless of the nature of the end-group, see Figure 2a. DLS was used to determine the intensity-average diameters of the three types of nanoparticles, which were in good agreement (see Figure 2b). Moreover, the nature of the end-group had minimal effect on the mean nanoparticle diameter, which is an important parameter for the formation of Pickering nanoemulsions using microfluidization.[25] As the nanoparticle dimensions and chemical compositions are very similar, this enables the effect of varying the nature of the end-group on the non-ionic steric stabilizer chains to be examined for this model system.

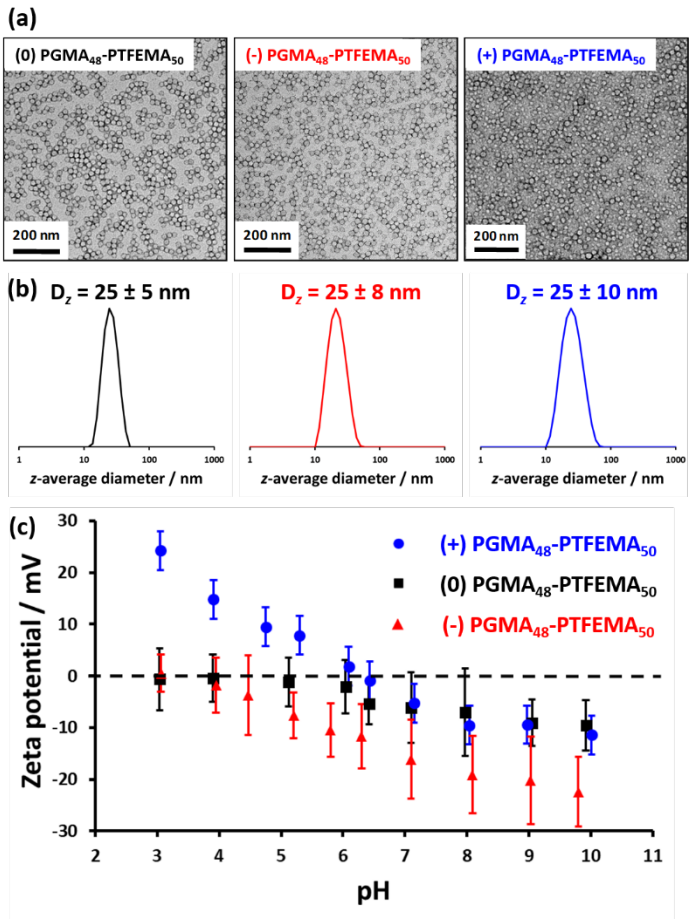

Figure 2. (a) Representative TEM images obtained for $PGMA_{48}$-$PTFEMA_{50}$ diblock copolymer nanoparticles prepared by RAFT aqueous emulsion polymerization of TFEMA, with the $PGMA_{48}$ precursor block synthesized using either CPDB (0), PETTC (-) or MPETTC (+) RAFT agents. (b) Corresponding DLS intensity-average size distributions and (c) Zeta potential *vs.* pH curves obtained for (0) $PGMA_{48}$-$PTFEMA_{50}$, (-) $PGMA_{48}$-$PTFEMA_{50}$ and (+) $PGMA_{48}$-$PTFEMA_{50}$ nanoparticles. Measurements are reported for 0.1% w/w copolymer dispersions prepared in the presence of 1 mM KCl. All pH titrations were performed from high pH to low pH. The error bars shown for the zeta potential data are equivalent to one standard deviation.

$PGMA_{48}$-$PTFEMA_{50}$ nanoparticles prepared using the PETTC RAFT agent bear carboxylic acid end-groups whereas the same nanoparticles prepared using MPETTC bear tertiary amine end-groups. Therefore, the solution pH at which the nanoemulsions are prepared is expected to influence the Pickering performance of these nanoparticles. Zeta potential measurements were performed to examine the effect of varying the solution pH on the aqueous electrophoretic behavior of the nanoparticles (Figure 2c). For (0) $PGMA_{48}$-$PTFEMA_{50}$ nanoparticles, a modest change in zeta potential from approximately zero to -12 mV was observed on raising the solution pH from 3 to 10. This weakly anionic character may

indicate the presence of carboxylic acid end-groups on some of the PGMA stabilizer chains originating from the ACVA initiator used for their RAFT syntheses. Alternatively, this anionic character may simply result from hydroxide ions adsorbing onto the surface of the nanoparticles at high pH.[70] In this context, it is perhaps noteworthy that the zeta potential of the (0) $PGMA_{48}$-$PTFEMA_{50}$ nanoparticles is comparable to that of (+) $PGMA_{48}$-$PTFEMA_{50}$ nanoparticles at pH 10.

In contrast, a much more significant change in zeta potential (from approximately zero to -25 mV) is observed for the (-) $PGMA_{48}$-$PTFEMA_{50}$ nanoparticles within the same pH range. The strongly anionic character observed at high pH indicates that the carboxylic acid end-groups are fully ionized under such conditions. This is consistent with observations reported by Lovett *et al*. for carboxylic acid-functionalized diblock copolymer worms, which underwent a worm-to-sphere transition on raising the solution pH solely as a result of end-group ionization.[59] Moreover, acid titration studies of a PETTC-derived (-) $PGMA_{56}$ macro-CTA indicated that the pK_a of its terminal carboxylic group was approximately 4.7.[59] This suggests that the negative zeta potentials observed for the (-) $PGMA_{48}$-$PTFEMA_{50}$ nanoparticles arise from such anionic end-groups.

For (+) $PGMA_{48}$-$PTFEMA_{50}$ nanoparticles, a significant increase in zeta potential from approximately zero to +25 mV occurs on lowering the solution pH from 6 to 3. These observations are consistent with aqueous electrophoresis data reported by Penfold *et al*. for morpholine-functionalized $PGMA_{50}$-$PHPMA_{140}$ diblock copolymer nano-objects.[61] The cationic zeta potentials observed on lowering the solution pH indicate protonation of the terminal morpholine group located on the $PGMA_{50}$ stabilizer chains, for which acid titration studies indicate a conjugate acid pK_a of approximately 6.3.[61] Thus, the aqueous electrophoretic behaviour of these three types of diblock copolymer nanoparticles can be adjusted simply by changing the solution pH.

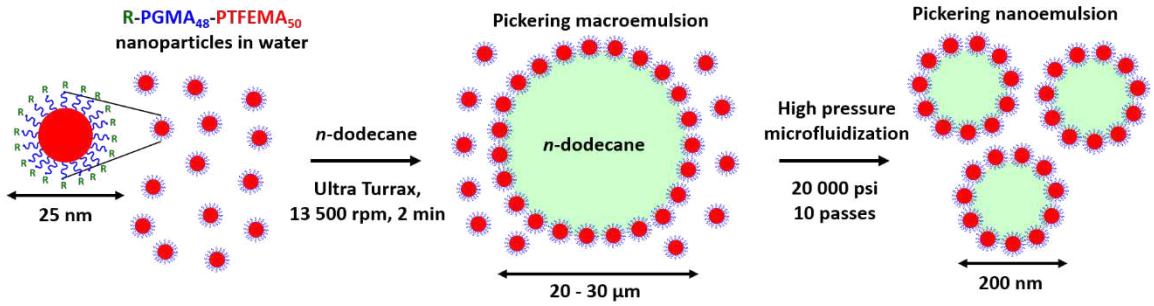

Figure 3. Schematic representation of the two-step preparation of Pickering nanoemulsions. First, a 7.0 % w/v aqueous dispersion of $PGMA_{48}$-$PTFEMA_{50}$ nanoparticles at either pH 3 or pH 7 are homogenized with *n*-dodecane to form an *n*-dodecane-in-water Pickering macroemulsion of around 20-30 µm diameter using conventional high-shear homogenisation at 13 500 rpm for 2 min at 20 °C. This relatively coarse precursor emulsion is then refined via ten passes through a commercial LV1 microfluidizer at 20 000 psi to obtain the final Pickering nanoemulsions of approximately 200 nm diameter that are used in this study. (See Figure 1 for details of each of the three terminal R groups on the end of the PGMA stabilizer chains).

Initially, 7.0% w/v aqueous dispersions of $PGMA_{48}$-$PTFEMA_{50}$ nanoparticles were prepared and the solution pH was adjusted to either 3 or 7 using 1 M HCl or NaOH, respectively. These dispersions were then used to prepare precursor Pickering macroemulsions with a mean droplet diameter of around 20-30 µm via high-shear homogenization. Such precursor macroemulsions were then processed using a commercial LV1 microfluidizer to produce Pickering nanoemulsions, see Figure 3. The latter step had been previously optimized by Thompson and co-workers, who found that a substantial excess of $PGMA_{48}$-$PTFEMA_{50}$ nanoparticles should be present after formation of the initial macroemulsion. This is because these non-adsorbed nanoparticles are required to stabilize the additional oil-water interface generated during high-pressure microfluidization.[25] Furthermore, it was empirically established that an applied pressure of 20 000 psi was optimal for the preparation of stable Pickering nanoemulsions.[25] Lower pressures led to larger, more polydisperse droplets, whereas higher pressures led to in situ dissociation of the $PGMA_{48}$-$PTFEMA_{50}$ nanoparticles to form individual diblock copolymer chains, which then acted as amphiphilic copolymer surfactant to form non-Pickering nanoemulsions.[25]

TEM images were obtained for dried fresh Pickering nanoemulsions, see Figure 4. Although the volatile droplet phase is no longer present under the ultrahigh vacuum conditions required for TEM, some of the original superstructure of the adsorbed $PGMA_{48}$-

PTFEMA$_{50}$ nanoparticles is preserved. Such *postmortem* studies suggest that spherical oil droplets with nanoscale dimensions corresponding to that indicated by DLS studies were indeed formed when using each of the three nanoparticles as a Pickering emulsifier. It is perhaps worth highlighting that no salt was added to these oil-in-water Pickering macroemulsions prior to their microfluidization. The hydrodynamic forces generated during this processing step are sufficient to form nanoemulsion droplets, despite the presence of charged end-groups on the steric stabilizer chains under certain conditions. Moreover, these TEM images provide a useful qualitative indication of the adsorption efficiency of these nanoparticle emulsifiers when varying the solution pH. More specifically, when the aqueous dispersion pH is adjusted to generate either cationic or anionic end-groups, fewer nanoparticles are adsorbed at the oil/water interface, so the fraction of free (non-adsorbed) nanoparticles increases (compare Figures 4d and 4e with Figures 4c and 4f, respectively). In order to confirm that these observations are not simply a drying artefact during the TEM sample preparation, nanoparticle adsorption efficiencies were determined quantitatively using GPC. In addition, these Pickering nanoemulsions were analyzed by SAXS.

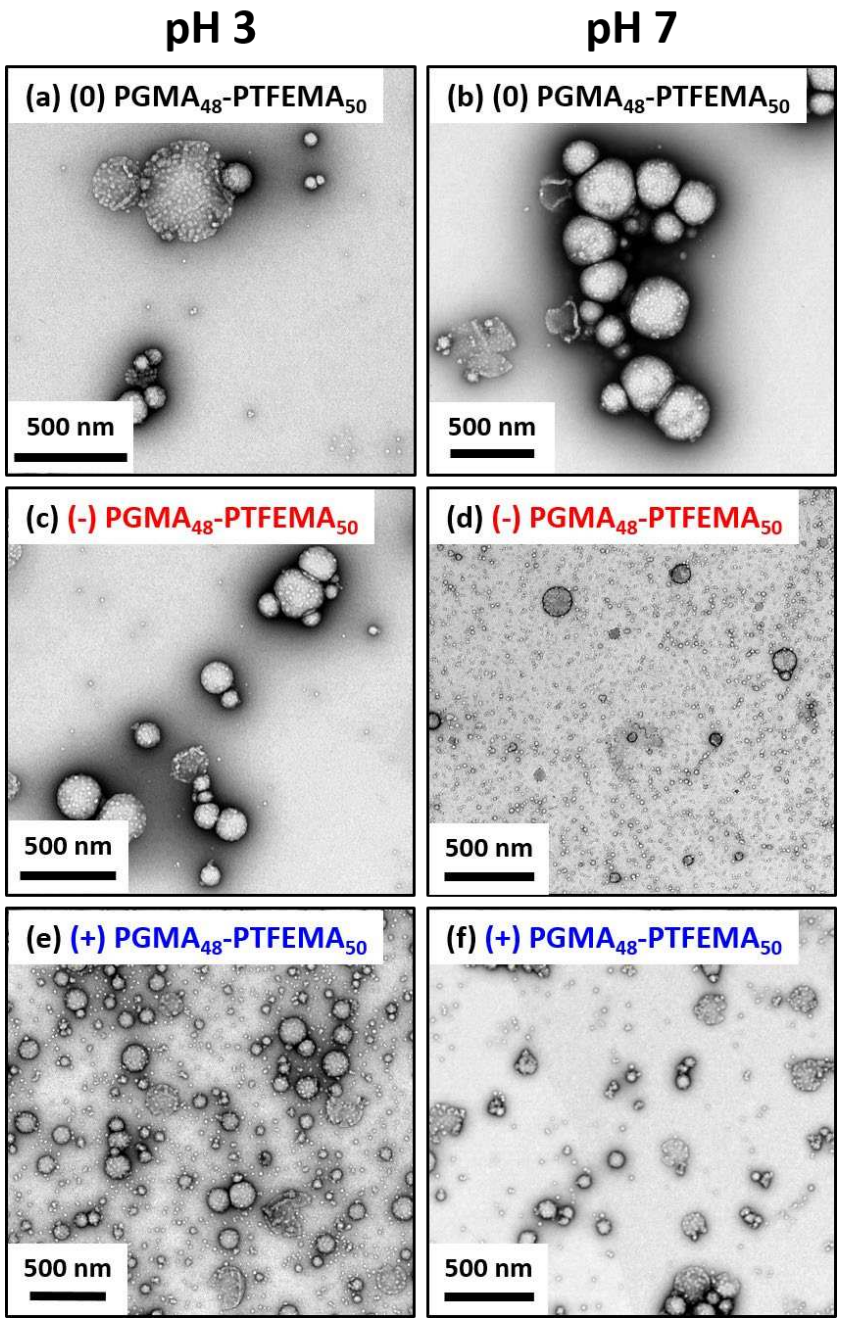

Figure 4. Representative TEM images obtained for dried *n*-dodecane-in-water Pickering nanoemulsions prepared with 7.0% w/w $PGMA_{48}$-$PTFEMA_{50}$ diblock copolymer nanoparticles synthesized using (a) CPDB at pH 3 (neutral); (b) CPDB at pH 7 (weakly anionic); (c) PETTC at pH 3 (neutral); (d) PETTC at pH 7 (strongly anionic); (e) MPETTC at pH 3 (strongly cationic); (f) MPETTC at pH 7 (neutral). The nanoemulsions were prepared using an LV1 microfluidizer at an applied pressure of 20 000 psi for 10 passes.

Table 1 summarizes the intensity-average droplet diameters, nanoparticle adsorption efficiencies and zeta potentials determined for freshly-prepared Pickering nanoemulsions using each of the three types of nanoparticles at either pH 3 or 7. DLS studies indicate that changing the aqueous dispersion pH prior to microfluidization leads to no systematic

variation in the initial droplet diameter. However, varying this parameter leads to the steric stabilizer chain-ends acquiring charge, which has a significant effect on the nanoparticle adsorption efficiency, packing efficiency and zeta potential of the Pickering nanoemulsions. For nanoemulsions prepared using (-) $PGMA_{48}$-PTFEMA nanoparticles, negative zeta potentials were obtained regardless of the pH. Thus a zeta potential of -7 mV is observed at pH 3 whereas at pH 7 the zeta potential is -48 mV, which is more than twice that of the nanoparticles alone at the same pH (–22 mV). This is attributed to the formation of anionic carboxylate end-groups on the PGMA steric stabilizer chains. In contrast, the (+) $PGMA_{48}$-$PTFEMA_{50}$-stabilized nanoemulsion exhibits minimal anionic character (-6 mV) at pH 7, whereas the zeta potential is strongly cationic (+27 mV) at pH 3 owing to protonation of the morpholine end-groups. This value is comparable to that exhibited by the (+) $PGMA_{48}$-$PTFEMA_{50}$ nanoparticles alone at the same pH (+24 mV).

Table 1. Summary of the Pickering nanoemulsions prepared using either (0) $PGMA_{48}$-$PTFEMA_{50}$, (-) $PGMA_{48}$-$PTFEMA_{50}$ or (+) $PGMA_{48}$-$PTFEMA_{50}$ diblock copolymer nanoparticles at either pH 3 or 7.

End-group type	pH 3				pH 7			
	DLS droplet diameter / nm	Adsorption efficiency / %	Packing efficiency / %	Zeta potential / mV	DLS droplet diameter / nm	Adsorption efficiency / %	Packing efficiency / %	Zeta potential / mV
Neutral	197 ± 56	93	49	0 ± 3	200 ± 72	90	47	-14 ± 4
Anionic	215 ± 74	90	52	-7 ± 4	212 ± 60	49	27	-48 ± 5
Cationic	198 ± 56	63	33	+27 ± 4	204 ± 61	93	50	-6 ± 5

The effect of varying the solution pH on the nanoparticle adsorption efficiency was assessed by GPC using a UV detector, see Table 1. Analysis of UV chromatograms recorded after serial dilution of the original aqueous nanoparticle dispersions enabled construction of a calibration plot of integrated UV signal against copolymer concentration at a wavelength of 298 nm (see Figure S3). This linear plot was used to quantify the concentration of non-adsorbed nanoparticles remaining in the aqueous phase after microfluidization (after using

centrifugation to remove the creamed oil droplets) and the extent of nanoparticle adsorption was calculated by difference. TEM studies suggest that there are far more non-adsorbed nanoparticles present in the aqueous phase when the nanoemulsion is prepared at pH 7 using (-) $PGMA_{48}$-$PTFEMA_{50}$ compared to the other two types of nanoparticles. This suggests that anionic end-groups reduce the extent of nanoparticle adsorption at the oil-water interface, which is in agreement with the nanoparticle adsorption efficiency determined using UV GPC. In a complementary experiment, the solution pH of each 7% w/w aqueous dispersion of nanoparticles was adjusted to pH 3 prior to homogenization. In this case, the adsorption efficiency of the (0) $PGMA_{48}$-$PTFEMA_{50}$ nanoparticles remained almost unchanged, whereas that of the carboxylic acid-functionalized (-) $PGMA_{48}$-$PTFEMA_{50}$ nanoparticles increased significantly from 49 % to 90 %. On the other hand, the efficiency of the morpholine-functionalized (+) $PGMA_{48}$-$PTFEMA_{50}$ nanoparticles was substantially reduced from 93 % to 63 %. Thus the introduction of surface charge clearly hinders efficient nanoparticle adsorption at the oil/water interface. It has been previously reported that both anionic[66-67, 71] and cationic[67] particles can be excluded from the oil/water interface owing to strong inter-particle repulsion, image charge effects,[67] and, in the case of anionic particles, like charges at the oil/water interface.[71] However, interfacial adsorption can be achieved by either adjusting the solution pH or increasing the ionic strength to suppress surface charge. In the current study, fewer nanoparticles are adsorbed at the oil/water interface during microfluidization if they possess cationic or anionic end-groups. This is because charged nanoparticles are more hydrophilic and thus are less strongly adsorbed at the oil/water interface.

As previously described, there is no discernible change in the intensity-average diameter of nanoemulsions at either pH 3 or 7. However, the nanoparticle adsorption efficiency differs significantly under such conditions. Since the volume of the oil phase is

equal in each case, this implies substantial differences in the nanoparticle packing efficiency at the surface of the oil droplets.

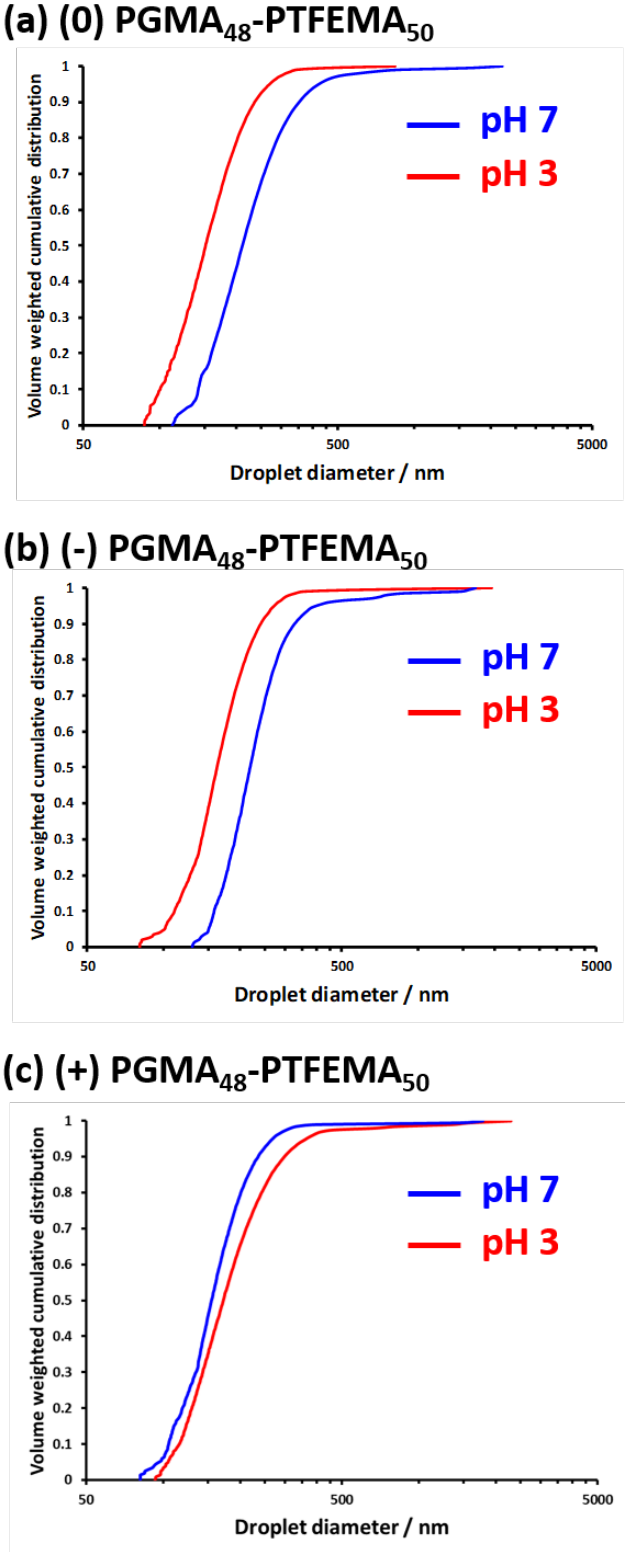

Figure 5. Volume-weighted cumulative size distributions determined by analytical centrifugation (LUMiSizer instrument) obtained for *n*-dodecane-in-water nanoemulsions prepared with 7.0% w/w $PGMA_{48}$-$PTFEMA_{50}$ diblock copolymer nanoparticles synthesized using: (a) CPDB (0), (b) PETTC (-) or (c) MPETTC (+) as the RAFT agent. Microfluidization conditions: applied pressure = 20 000 psi, ten passes and a solution pH of either 3 or 7.

Figure 5 shows volume-average cumulative size distributions recorded for each of the freshly-made nanoemulsions prepared at either pH 3 or 7, as determined by analytical centrifugation. In contrast to the intensity-average size distributions reported by DLS, there are clear differences in size for Pickering nanoemulsions prepared at pH 3 and pH 7. As noted by Thompson and co-workers, analytical centrifugation has a much higher resolution compared to DLS because droplet fractionation occurs prior to detection.[27] However, one drawback of the former technique is that the *effective particle density* is required to obtain an accurate particle size.[45] This parameter was estimated to be 0.81 g cm^{-3} for a $PGMA_{48}$-$PTFEMA_{50}$ stabilized *n*-dodecane-in-water nanoemulsion. This value is higher than that of *n*-dodecane (0.75 g cm^{-3}) because the nanoparticle density is 1.15 g cm^{-3}, as previously determined by Akpinar and co-workers.[45] Moreover, undersizing can be observed if the droplet concentration is too high owing to the phenomenon of hindered creaming.[27, 75] However, using droplet concentrations that are too low is also problematic: such dilute emulsions scatter light only rather weakly and hence fall outside of the optimum transmission range required for the LUMiSizer instrument (i.e. below 30 % transmission). Given these conflicting requirements, a droplet concentration of 1.0% v/v was found to be optimum.[25] In the current study, this concentration was used for all analytical centrifugation measurements. A further complication for this sizing technique is that a density distribution is superimposed on the droplet size distribution, as discussed by Thompson and co-workers.[27] Overall, this means that analytical centrifugation is best utilized for monitoring *relative* changes in the droplet size distribution during long-term ageing of these Pickering nanoemulsions, rather than for determining *absolute* droplet diameters.

The volume-average cumulative size distributions shown in Figure 5 demonstrate that Pickering nanoemulsions prepared using nanoparticles that possess charged end-groups leads

to the formation of larger, more polydisperse droplets. For example, nanoemulsions prepared using (-) $PGMA_{48}$-$PTFEMA_{50}$ nanoparticles exhibited an initial volume-average droplet diameter of 159 ± 54 nm at pH 3, whereas nanoemulsions prepared using the same nanoparticles at pH 7 had a significantly larger droplet diameter of 218 ± 169 nm. This size difference can be correlated with the substantially different nanoparticle adsorption efficiencies noted above. More specifically, only 49% of the (-) $PGMA_{48}$-$PTFEMA_{50}$ nanoparticles are adsorbed on the surface of the oil droplets at pH 7 compared to 90% at pH 3. Because there are far fewer nanoparticles adsorbed at the oil/water interface at pH 7, only relatively large oil droplets can be stabilized at the same copolymer concentration. A similar effect is observed for (+) $PGMA_{48}$-$PTFEMA_{50}$ nanoparticles. Protonation of the morpholine end-groups at pH 3 leads to a 30% reduction in nanoparticle adsorption efficiency compared to the neutral form of such nanoparticles at pH 7. Thus interfacial adsorption of the nanoparticles is again suppressed, despite the favourable electrostatic attraction between the cationic nanoparticles and the anionic oil/water interface. These results demonstrate the importance of the choice of RAFT agent (which dictates the nature of the stabilizer end-groups) when designing diblock copolymer nanoparticles for use as Pickering emulsifiers.

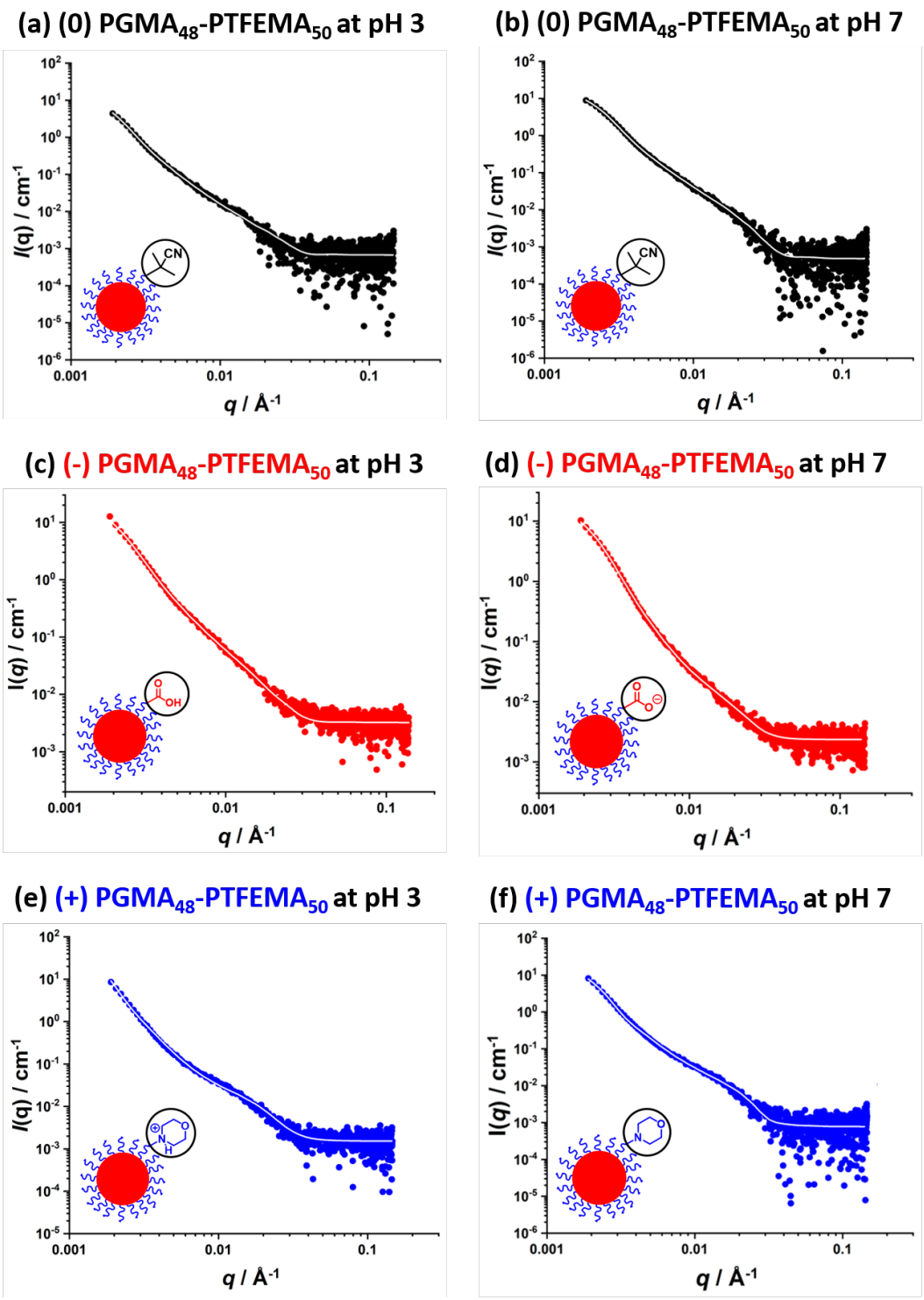

Figure 6. Experimental SAXS patterns (circles) and calculated data fits (white lines) obtained for 1.0% v/v nanoemulsions prepared using (a) CPDB at pH 3 (neutral nanoparticles); (b) CPDB at pH 7 (weakly anionic nanoparticles); (c) PETTC at pH 3 (neutral nanoparticles); (d) PETTC at pH 7 (strongly anionic nanoparticles); (e) MPETTC at pH 3 (strongly cationic nanoparticles); (f) MPETTC at pH 7 (neutral nanoparticles). Each nanoemulsion was prepared using an LV1 microfluidizer at an applied pressure of 20 000 psi for ten passes. The two-population core-shell structural model used for the SAXS analysis of such Pickering nanoemulsions comprises large oil droplet cores coated with a layer (or shell) of adsorbed spherical nanoparticles.

TEM studies suggest that these Pickering nanoemulsions possess a core-shell morphology with a particulate shell. However, this technique cannot be used to assess the surface coverage of the *n*-dodecane droplets by the adsorbed layer of nanoparticles. Prior studies indicate that scattering techniques should provide useful information in this context.[76] Thus, SAXS patterns were recorded for freshly-prepared Pickering nanoemulsions after dilution to 1.0% v/v (Figure 6). Following our prior study of the characterization of core-shell nanocomposite particles comprising polymer latex cores and particulate silica shells,[77] the SAXS data were analyzed using a two-population model. Population 1 of the model is represented by core-shell spheres, where the cores comprise the oil droplets and the adsorbed layer of nanoparticles form the shell. The particulate nature of the shell is described by small homogeneous spheres corresponding to population 2. First, SAXS patterns recorded for the nanoparticles alone (see Figure S4) were fitted using a spherical form factor[78]. The resulting mean particle radius (R_s) and its associated standard deviation (σ_s) (Table 2) were consistent with those obtained by DLS and TEM studies (Figure 2). These two parameters were subsequently fixed when fitting the SAXS patterns of the Pickering nanoemulsions using the two-population model (see Table 2). The scattering length density for each component of the Pickering nanoemulsions [oil core (ξ_c), particulate shell (ξ_{shell}) and surrounding liquid ($\xi_{solvent}$)] was calculated based on their respective known chemical compositions and mass densities (Table 2). These three parameters were also fixed for the subsequent SAXS data fitting. The packing efficiency for the nanoparticles within the particulate shell surrounding the oil droplets was included in such calculations (see Table 3). The structure of these Pickering nanoemulsions can be described by the mean core radius (R_c) and its standard deviation (σ_c), the mean shell thickness (T_s), and two scaling factors (for the core-shell particles and the copolymer nanoparticles, respectively). These five parameters were allowed to vary during fitting the SAXS data.

SAXS patterns for the nanoemulsions comprised three distinct regions: (i) relatively intense scattering at low q arising from the nanoemulsion droplets (where close inspection reveals a subtle change in gradient at low q, indicating cross-over from the Porod region to the Guinier region); (ii) additional scattering intensity at intermediate q corresponding to the copolymer nanoparticle form factor (Figure S4) and (iii) relatively weak scattering at high q, which is most likely associated with thermal fluctuations in the oil density and copolymer components (accordingly, constant background scattering has been incorporated into the model to account for this feature). The two-population model produced a reasonably good fit to the experimental SAXS pattern obtained for each Pickering nanoemulsion. The lack of well-defined minima in these scattering curves suggests that the nanoemulsion droplets are somewhat polydisperse in terms of their size, which is consistent with TEM and DLS studies. Mean droplet radii calculated using the two-population model (Table 2) were consistent with those reported by DLS and analytical centrifugation (Table 1 and Figure 5, respectively). However, these values are not particularly accurate owing to our laboratory-based SAXS instrument, which has limited resolution at low q. The mean apparent thickness of the shell of adsorbed nanoparticles calculated for these Pickering nanoemulsions was approximately 12-15 nm in each case, which is less than the mean diameter of an individual nanoparticle (~ 22 nm, Table 2). This is reasonably consistent with the relatively low surface coverage of the oil droplets by the nanoparticles, which exhibit packing efficiencies of 27-52% (Table 1). Furthermore, T_s varied with solution pH for the Pickering nanoemulsions prepared with (-) and (+) $PGMA_{48}$-$PTFEMA_{50}$ nanoparticles (Table 2). For example, T_s was calculated to be 11.9 nm for nanoemulsions prepared using (-) $PGMA_{48}$-$PTFEMA_{50}$ nanoparticles at pH 7, whereas those prepared using the same nanoparticles at pH 3 had a significantly thicker shell of 14.7 nm. This is consistent with a higher packing efficiency under the latter conditions, when the nanoparticles are in their neutral form (Table 1). In contrast, T_s *decreases* for the (+)

$PGMA_{48}$-$PTFEMA_{50}$ nanoparticles on switching from pH 7 to pH 3 (Table 2). In contrast, the T_s values determined for Pickering nanoemulsions stabilized using the neutral nanoparticles are essentially independent of solution pH, indicating no significant change in the nanoparticle packing efficiency under such conditions.

Table 2. Structural parameters obtained by SAXS analysis of 1.0% v/v Pickering nanoemulsions comprising *n*-dodecane droplets prepared using either neutral $PGMA_{48}$-$PTFEMA_{50}$, anionic $PGMA_{48}$-$PTFEMA_{50}$ or cationic $PGMA_{48}$-$PTFEMA_{50}$ nanoparticles at either pH 3 or pH 7.[a]

End-group type	pH 3				pH 7			
	R_c / nm	σ_c / nm	T_s / nm	ξ_{shell} x 10^{10} cm^{-2}	R_c / nm	σ_c / nm	T_s / nm	ξ_{shell} x 10^{10} cm^{-2}
Neutral	127	41	14.9	10.85	118	35	14.4	10.79
Anionic	104	41	14.7	10.93	94	36	11.9	10.21
Cationic	162	47	12.2	10.38	128	32	14.2	10.88

[a] R_c = mean core radius; σ_c = standard deviation of the core radius; T_s = mean shell thickness; ξ_{shell} = effective scattering length density of the particulate shell; R_s = copolymer nanoparticle radius, σ_s = standard deviation of the copolymer nanoparticle radius. Parameters used for modeling are as follows: $\xi_{solvent}$ = 9.42 x 10^{10} cm^{-2}; ξ_c = 7.32 x 10^{10} cm^{-2}; neutral R_s = 10.7 nm, σ_s = 1.3; anionic R_s = 11.4 nm, σ_s = 2.5 , cationic R_s = 11.4 nm, σ_s = 2.5. The ξ_{shell} was calculated by averaging the scattering length densities of the PGMA stabilizer block (11.94 x 10^{10} cm^{-2}), the PTFEMA core-forming block (12.76 x 10^{10} cm^{-2}) and the solvent (water) based on the copolymer composition and packing efficiency of the copolymer nanoparticles on the oil droplets.

To examine the effect of the stabilizer end-groups on the long-term stability of the nanoemulsions, analytical centrifugation was used to determine the mean droplet size after ageing for both one week and six weeks at 20 °C. Volume-weighted cumulative size distributions for freshly-made and one-week-old nanoemulsions at pH 7 and pH 3 are shown in Figure 7. Nanoemulsions stabilized by nanoparticles with anionic or cationic end-groups (see Figure 7b and 7c) displayed the greatest rate of droplet growth within one week.

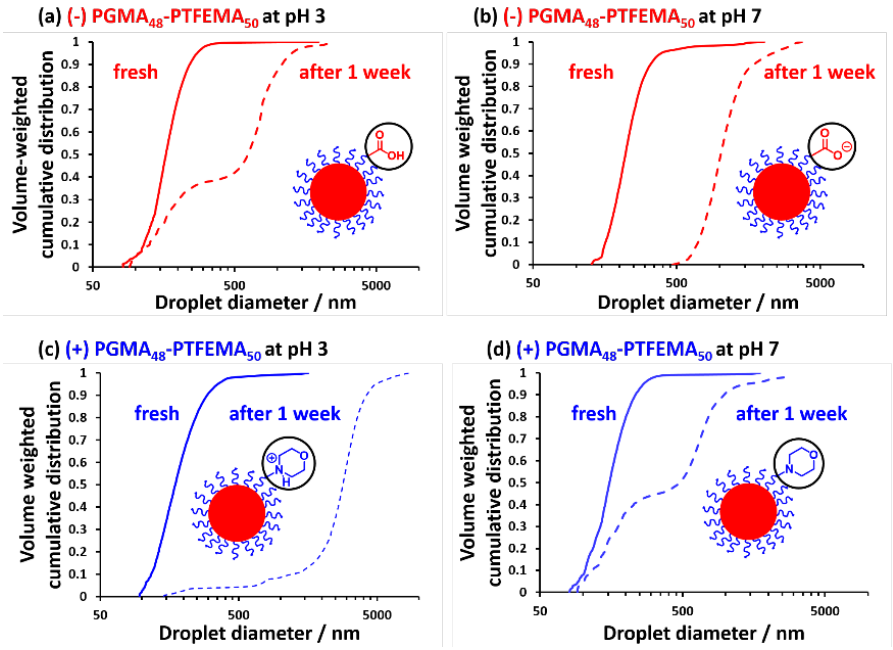

Figure 7. Volume-weighted cumulative size distributions determined by analytical centrifugation (LUMiSizer instrument) for fresh (solid line) and aged (for one week at 20 °C, dashed line) *n*-dodecane-in-water Pickering nanoemulsions prepared using 7.0% w/w $PGMA_{48}$-$PTFEMA_{50}$ diblock copolymer nanoparticles synthesized with the following RAFT agents: (a) PETTC, aged at pH 3; (b) PETTC, aged at pH 7; (c) MPETTC, aged at pH 3; (d) MPETTC, aged at pH 7. Microfluidizer conditions: 20 000 psi; ten passes

The droplet size distributions of such aged nanoemulsions are relatively unimodal. In contrast, nanoemulsions stabilized by nanoparticles prepared with neutral end-groups (see Figures 6a and 6d) possess distinctly bimodal size distributions after ageing for one week, with the minor population corresponding to the original droplets. The extent of Ostwald ripening is similar for nanoemulsions stabilized by either (+) $PGMA_{48}$-$PTFEMA_{50}$ or (-) $PGMA_{48}$-$PTFEMA_{50}$: around 60% of the oil droplets exceed approximately 500 nm after ageing for one week at 20 °C. As shown above, using neutral nanoparticles as Pickering emulsifiers leads to adsorption efficiencies of around 90%. According to UV GPC studies, the nanoparticle adsorption efficiency for the charged nanoparticles is significantly lower than that for the corresponding neutral nanoparticles. Moreover, a somewhat lower droplet surface coverage is anticipated in the former case because of lateral electrostatic repulsion between neighbouring adsorbed nanoparticles: this is also expected to facilitate faster droplet growth via coalescence.[79] In practice, the calculated packing efficiencies for anionic or

cationic nanoparticles adsorbed onto the oil droplets are 27% or 33% respectively, which are significantly lower than those observed for the adsorbed neutral nanoparticles (~ 47-49%) (Table 1). Such lower surface coverages mean that the adsorbed layers of charged nanoparticles provide a somewhat less effective barrier against *n*-dodecane diffusion into the aqueous phase.[31] Thus, the corresponding nanoemulsions exhibit inferior long-term stability with respect to droplet coalescence.[69, 80-81] Similar observations have been reported in the literature for surfactant-stabilized nanoemulsions.[82] Analytical centrifugation studies of the evolution of droplet size distributions over time enables both the extent and mechanism of droplet growth to be assessed. According to the literature, it is generally accepted that the main destabilization mechanism for nanoemulsions is Ostwald ripening,[24-25, 27, 31, 40-41] which is characterized by a linear increase in the cube of the mean droplet radius over time.[83-84] Analytical centrifugation was used to monitor droplet coarsening over time for the Pickering nanoemulsion prepared using the (-) $PGMA_{48}$-$PTFEMA_{50}$ nanoparticles. This technique indicated that the initial unimodal droplet size distribution gradually developed bimodal character. Nevertheless, a linear relationship was observed when plotting the cube of the volume-average droplet radius against ageing time at either pH 3 or pH 7 (see Figure S5), which is consistent with the expected Ostwald ripening mechanism.

Table 3. Variation in Mean Droplet Diameter with Ageing Time as Determined by Analytical Centrifugation for Pickering Nanoemulsions Stabilized using Nanoparticles with either Neutral, Anionic or Cationic End-Groups

End-group type	Mean droplet diameter determined by analytical centrifugation (nm)					
	pH 3			pH 7		
	fresh	1 week	6 weeks	fresh	1 week	6 weeks
Neutral	176 ± 130	177 ± 142	177 ± 419	207 ± 162	208 ± 314	184 ± 411
Anionic	159 ± 108	292 ± 425	868 ± 1326	218 ± 169	1005 ± 524	2017 ± 886
Cationic	171 ± 136	1283 ± 1691	1937 ± 2938	140 ± 118	257 ± 500	323 ± 1246

Table 3 reports the mean volume-average droplet diameter determined by analytical centrifugation for Pickering nanoemulsions prepared using each of the three types of nanoparticles after ageing for up to six weeks at 20 °C. In each case, there is evidence for Ostwald ripening but nanoemulsions prepared using nanoparticles bearing charged end-groups undergo substantially greater ripening compared to those prepared using approximately neutral nanoparticles. Nanoparticles prepared using the CPDB RAFT agent formed the most stable nanoemulsions: the mean droplet diameter actually remains roughly constant but the width of the size distribution increases significantly. Nanoemulsions prepared using (+) $PGMA_{48}$-$PTFEMA_{50}$ nanoparticles at pH 3 grew from 171 ± 135 μm to 1937 ± 2938 μm, whereas the mean droplet diameter only increased from 140 ± 118 μm to 323 ± 1246 μm at pH 7. Perhaps surprisingly, nanoemulsions prepared using the (-) $PGMA_{48}$-$PTFEMA_{50}$ nanoparticles proved to be relatively unstable with respect to ageing regardless of the solution pH. Overall, it is clear that using charged nanoparticles as Pickering emulsifiers produces nanoemulsions with inferior long-term stability. Interestingly, the nanoemulsion zeta potential cannot be used to reliably predict the long-term stability of such Pickering nanoemulsions.

CONCLUSIONS

The effect of charged end-groups on the formation and long-term stability of Pickering nanoemulsions has been explored using model sterically-stabilized diblock copolymer nanoparticles prepared by polymerization-induced self-assembly. More specifically, such nanoparticles were prepared by chain-extending a water-soluble non-ionic $PGMA_{48}$ precursor via RAFT aqueous emulsion polymerization of TFEMA to produce well-defined spherical nanoparticles of approximately 20 nm diameter in each case, as judged by DLS, TEM and

SAXS studies. Aqueous electrophoresis studies indicated that nanoparticles prepared using PGMA chains with a terminal carboxylic acid end-group displayed strong anionic character at pH 7, whereas those containing a terminal tertiary amine end-group exhibited strong cationic character at pH 3. On the other hand, nanoparticles prepared using a neutral RAFT agent displayed only weakly anionic character at pH 7, most likely owing to hydroxide ion adsorption. These three types of sterically-stabilized nanoparticles were used in turn to prepare *n*-dodecane-in-water nanoemulsions via high-pressure microfluidization at either pH 3 or pH 7. DLS studies confirmed that mean droplet diameters of approximately 200 nm can be readily obtained. TEM studies indicated that the nanoparticle superstructure remained intact on drying, thus providing evidence for the Pickering nature of these nanoemulsions. Mean droplet diameters obtained for the fresh nanoemulsions using analytical centrifugation were all equal to or less than 200 nm. UV GPC analysis of the aqueous phase enabled quantification of the excess non-adsorbed nanoparticles. In the absence of any charged end-groups, the nanoparticle adsorption efficiency was calculated to be approximately 90%. However, the presence of charged end-groups significantly reduced the nanoparticle adsorption efficiency because electrostatic repulsions between neighboring copolymer nanoparticles suppresses their interfacial adsorption and reduces their packing efficiency at the oil-water interface. This was confirmed by analyzing SAXS patterns recorded for the Pickering nanoemulsions using a two-population model. Furthermore, long-term stability studies using analytical centrifugation revealed significantly faster droplet coarsening via Ostwald ripening for the latter Pickering nanoemulsions compared to those prepared using neutral nanoparticles under comparable conditions. This was attributed to the lower packing efficiencies for oil droplets stabilized by nanoparticles bearing charged end-groups compared to those observed for neutral nanoparticles.

ASSOCIATED CONTENT

Supporting Information

^{19}F NMR spectra recorded for $PGMA_{48}$-$PTFEMA_{50}$ diblock copolymers; gel permeation chromatograms recorded for $PGMA_{48}$-$PTFEMA_{50}$ diblock copolymers; UV GPC calibration plot constructed for $PGMA_{48}$-$PTFEMA_{50}$ diblock copolymers bearing either neutral, carboxylic acid or tertiary amine end-groups; small-angle X-ray scattering patterns constructed for $PGMA_{48}$-$PTFEMA_{50}$ diblock copolymers bearing either neutral, carboxylic acid or tertiary amine end-groups at either pH 3 or 7; analytical centrifugation data recorded for one of the aged nanoemulsions.

This material is available free of charge via the Internet at http//:pubs.acs.org.

AUTHOR INFORMATION

Corresponding Authors

*Email s.p.armes@shef.ac.uk (S.P.A.)

The manuscript was written through contributions of all authors. All authors have given approval to the final version of the manuscript.

Funding Sources: EPSRC and DSM (Geleen, The Netherlands).

ACKNOWLEDGMENTS

EPSRC is thanked for a CDT PhD studentship to support S.J.H. (EP/L016281) and also an Established Career Particle Technology Fellowship (EP/ R003009) for S.P.A. DSM (Geleen, The Netherlands) is acknowledged for partial support of this PhD project and for permission to publish this work. S.P.A. and O.O.M. are grateful to EPSRC for a capital equipment grant to purchase the Xenocs/Excillum SAXS laboratory beamline (EP/M028437/1). The authors

thank Christopher Hill and Dr. Svetomir Tzokov at the University of Sheffield Biomedical Science Electron Microscopy suite.

REFERENCES

1. Ramsden, W., Separation of Solids in the Surface-Layers of Solutions and 'Suspensions' (Observations on Surface-Membranes, Bubbles, Emulsions, and Mechanical Coagulation). -- Preliminary Account. *Proc. R. Soc. London* **1903,** *72*, 156-164.

2. Pickering, S. U., Emulsions. *J. Chem. Soc.* **1907,** *91*, 2001-2021.

3. P. Binks, B.; O. Lumsdon, S., Stability of oil-in-water emulsions stabilised by silica particles. *Phys. Chem. Chem. Phys.* **1999,** *1*, 3007-3016.

4. Binks, B. P.; Whitby, C. P., Silica Particle-Stabilized Emulsions of Silicone Oil and Water: Aspects of Emulsification. *Langmuir* **2004,** *20*, 1130-1137.

5. Ikem, V. O.; Menner, A.; Bismarck, A., High-Porosity Macroporous Polymers Sythesized from Titania-Particle-Stabilized Medium and High Internal Phase Emulsions. *Langmuir* **2010,** *26*, 8836-8841.

6. Ashby, N. P.; Binks, B. P., Pickering emulsions stabilised by Laponite clay particles. *Phys. Chem. Chem. Phys.* **2000,** *2*, 5640-5646.

7. Kalashnikova, I.; Bizot, H.; Bertoncini, P.; Cathala, B.; Capron, I., Cellulosic nanorods of various aspect ratios for oil in water Pickering emulsions. *Soft Matter* **2013,** *9*, 952-959.

8. Kalashnikova, I.; Bizot, H.; Cathala, B.; Capron, I., New Pickering Emulsions Stabilized by Bacterial Cellulose Nanocrystals. *Langmuir* **2011,** *27*, 7471-7479.

9. Binks, B. P.; Murakami, R.; Armes, S. P.; Fujii, S., Temperature-Induced Inversion of Nanoparticle-Stabilized Emulsions. *Angew. Chem.* **2005,** *117*, 4873-4876.

10. Thompson, K. L.; Chambon, P.; Verber, R.; Armes, S. P., Can Polymersomes Form Colloidosomes? *J. Am. Chem. Soc.* **2012,** *134*, 12450-12453.

11. Binks, B. P., Particles as surfactants—similarities and differences. *Curr. Opin. Colloid Interface Sci.* **2002,** *7*, 21-41.

12. Cunningham, V. J.; Alswieleh, A. M.; Thompson, K. L.; Williams, M.; Leggett, G. J.; Armes, S. P.; Musa, O. M., Poly(glycerol monomethacrylate)–Poly(benzyl methacrylate) Diblock Copolymer Nanoparticles via RAFT Emulsion Polymerization: Synthesis, Characterization, and Interfacial Activity. *Macromolecules* **2014,** *47*, 5613-5623.

13. Thompson, K. L.; Fielding, L. A.; Mykhaylyk, O. O.; Lane, J. A.; Derry, M. J.; Armes, S. P., Vermicious thermo-responsive Pickering emulsifiers. *Chem. Sci.* **2015,** *6*, 4207-4214.

14. Thompson, K. L.; Lane, J. A.; Derry, M. J.; Armes, S. P., Non-aqueous Isorefractive Pickering Emulsions. *Langmuir* **2015,** *31*, 4373-4376.

15. Nguyen, B. T.; Wang, W.; Saunders, B. R.; Benyahia, L.; Nicolai, T., pH-Responsive Water-in-Water Pickering Emulsions. *Langmuir* **2015,** *31*, 3605-3611.

16. Nicolai, T.; Murray, B., Particle stabilized water in water emulsions. *Food Hydrocolloids* **2017,** *68*, 157-163.

17. Binks, B. P., Colloidal Particles at a Range of Fluid–Fluid Interfaces. *Langmuir* **2017,** *33*, 6947-6963.

18. Rozynek, Z.; Bielas, R.; Jozefczak, A., Efficient formation of oil-in-oil Pickering emulsions with narrow size distributions by using electric fields. *Soft Matter* **2018**.

19. Binks, B. P.; Lumsdon, S. O., Influence of Particle Wettability on the Type and Stability of Surfactant-Free Emulsions. *Langmuir* **2000,** *16*, 8622-8631.

20. Binks, B. P.; Olusanya, S. O., Pickering emulsions stabilized by coloured organic pigment particles. *Chem. Sci.* **2017,** *8*, 708-723.

21. Binks, B. P.; Lumsdon, S. O., Catastrophic Phase Inversion of Water-in-Oil Emulsions Stabilized by Hydrophobic Silica. *Langmuir* **2000,** *16*, 2539-2547.

22. Sacanna, S.; Kegel, W. K.; Philipse, A. P., Thermodynamically Stable Pickering Emulsions. *Phys. Rev. Lett.* **2007,** *98*, 158301.

23. Sihler, S.; Schrade, A.; Cao, Z.; Ziener, U., Inverse Pickering Emulsions with Droplet Sizes below 500 nm. *Langmuir* **2015,** *31*, 10392-10401.

24. Persson, K. H.; Blute, I. A.; Mira, I. C.; Gustafsson, J., Creation of well-defined particle stabilized oil-in-water nanoemulsions. *Colloids Surf., A* **2014,** *459*, 48-57.

25. Thompson, K. L.; Cinotti, N.; Jones, E. R.; Mable, C. J.; Fowler, P. W.; Armes, S. P., Bespoke Diblock Copolymer Nanoparticles Enable the Production of Relatively Stable Oil-in-Water Pickering Nanoemulsions. *Langmuir* **2017,** *33*, 12616-12623.

26. Jiménez Saelices, C.; Capron, I., Design of Pickering Micro- and Nanoemulsions Based on the Structural Characteristics of Nanocelluloses. *Biomacromolecules* **2018,** *19*, 460-469.

27. Thompson, K. L.; Derry, M. J.; Hatton, F. L.; Armes, S. P., Long-Term Stability of n-Alkane-in-Water Pickering Nanoemulsions: Effect of Aqueous Solubility of Droplet Phase on Ostwald Ripening. *Langmuir* **2018,** *34*, 9289-9297.

28. Kang, D. J.; Bararnia, H.; Anand, S., Synthesizing Pickering Nanoemulsions by Vapor Condensation. *ACS Applied Materials & Interfaces* **2018,** *10*, 21746-21754.

29. Du, Z.; Li, Q.; Li, J.; Su, E.; Liu, X.; Wan, Z.; Yang, X., Self-Assembled Egg Yolk Peptide Micellar Nanoparticles as a Versatile Emulsifier for Food-Grade Oil-in-Water Pickering Nanoemulsions. *J Agr Food Chem* **2019**.

30. Dieng, S. M.; Anton, N.; Bouriat, P.; Thioune, O.; Sy, P. M.; Massaddeq, N.; Enharrar, S.; Diarra, M.; Vandamme, T., Pickering nano-emulsions stabilized by solid lipid nanoparticles as a temperature sensitive drug delivery system. *Soft Matter* **2019**.

31. Solans, C.; Izquierdo, P.; Nolla, J.; Azemar, N.; Garcia-Celma, M. J., Nano-emulsions. *Curr. Opin. Colloid Interface Sci.* **2005,** *10*, 102-110.

32. McClements, D. J., Nanoemulsions versus microemulsions: terminology, differences, and similarities. *Soft Matter* **2012,** *8*, 1719-1729.

33. Sonneville-Aubrun, O.; Simonnet, J. T.; L'Alloret, F., Nanoemulsions: a new vehicle for skincare products. *Adv. Colloid Interface Sci.* **2004,** *108-109*, 145-149.

34. Rapoport, N. Y.; Kennedy, A. M.; Shea, J. E.; Scaife, C. L.; Nam, K.-H., Controlled and targeted tumor chemotherapy by ultrasound-activated nanoemulsions/microbubbles. *J Control Release* **2009,** *138*, 268-276.

35. Singh, Y.; Meher, J. G.; Raval, K.; Khan, F. A.; Chaurasia, M.; Jain, N. K.; Chourasia, M. K., Nanoemulsion: Concepts, development and applications in drug delivery. *J Control Release* **2017,** *252*, 28-49.

36. McClements, D. J.; Rao, J., Food-Grade Nanoemulsions: Formulation, Fabrication, Properties, Performance, Biological Fate, and Potential Toxicity. *Critical Reviews in Food Science and Nutrition* **2011,** *51*, 285-330.

37. McClements, D. J., Edible nanoemulsions: fabrication, properties, and functional performance. *Soft Matter* **2011,** *7*, 2297-2316.

38. Du, Z.; Wang, C.; Tai, X.; Wang, G.; Liu, X., Optimization and Characterization of Biocompatible Oil-in-Water Nanoemulsion for Pesticide Delivery. *ACS Sustainable Chemistry & Engineering* **2016,** *4*, 983-991.

39. Santos, J.; Trujillo-Cayado, L. A.; Calero, N.; Alfaro, M. C.; Muñoz, J., Development of eco-friendly emulsions produced by microfluidization technique. *Journal of Industrial and Engineering Chemistry* **2016,** *36*, 90-95.

40. Gupta, A.; Eral, H. B.; Hatton, T. A.; Doyle, P. S., Nanoemulsions: formation, properties and applications. *Soft Matter* **2016,** *12*, 2826-2841.

41. Rodriguez-Lopez, G.; O'Neil Williams, Y.; Toro-Mendoza, J., Individual and Collective Behavior of Emulsion Droplets Undergoing Ostwald Ripening. *Langmuir* **2019,** *35*, 5316-5323.

42. Canning, S. L.; Smith, G. N.; Armes, S. P., A Critical Appraisal of RAFT-Mediated Polymerization-Induced Self-Assembly. *Macromolecules* **2016,** *49*, 1985-2001.

43. Jones, E. R.; Semsarilar, M.; Blanazs, A.; Armes, S. P., Efficient Synthesis of Amine-Functional Diblock Copolymer Nanoparticles via RAFT Dispersion Polymerization of Benzyl Methacrylate in Alcoholic Media. *Macromolecules* **2012,** *45*, 5091-5098.

44. Warren, N. J.; Armes, S. P., Polymerization-Induced Self-Assembly of Block Copolymer Nano-objects via RAFT Aqueous Dispersion Polymerization. *J. Am. Chem. Soc.* **2014,** *136*, 10174-10185.

45. Akpinar, B.; Fielding, L. A.; Cunningham, V. J.; Ning, Y.; Mykhaylyk, O. O.; Fowler, P. W.; Armes, S. P., Determining the Effective Density and Stabilizer Layer Thickness of Sterically Stabilized Nanoparticles. *Macromolecules* **2016,** *49*, 5160-5171.

46. Hatton, F. L.; Lovett, J. R.; Armes, S. P., Synthesis of well-defined epoxy-functional spherical nanoparticles by RAFT aqueous emulsion polymerization. *Polym. Chem.* **2017,** *8*, 4856-4868.

47. Ferguson, C. J.; Hughes, R. J.; Pham, B. T. T.; Hawkett, B. S.; Gilbert, R. G.; Serelis, A. K.; Such, C. H., Effective ab Initio Emulsion Polymerization under RAFT Control. *Macromolecules* **2002,** *35*, 9243-9245.

48. Ferguson, C. J.; Hughes, R. J.; Nguyen, D.; Pham, B. T. T.; Gilbert, R. G.; Serelis, A. K.; Such, C. H.; Hawkett, B. S., Ab Initio Emulsion Polymerization by RAFT-Controlled Self-Assembly. *Macromolecules* **2005,** *38*, 2191-2204.

49. Ganeva, D. E.; Sprong, E.; de Bruyn, H.; Warr, G. G.; Such, C. H.; Hawkett, B. S., Particle Formation in ab Initio RAFT Mediated Emulsion Polymerization Systems. *Macromolecules* **2007,** *40*, 6181-6189.

50. Chaduc, I.; Crepet, A.; Boyron, O.; Charleux, B.; D'Agosto, F.; Lansalot, M., Effect of the pH on the RAFT Polymerization of Acrylic Acid in Water. Application to the Synthesis of Poly(acrylic acid)-Stabilized Polystyrene Particles by RAFT Emulsion Polymerization. *Macromolecules* **2013,** *46*, 6013-6023.

51. Chaduc, I.; Zhang, W.; Rieger, J.; Lansalot, M.; D'Agosto, F.; Charleux, B., Amphiphilic Block Copolymers from a Direct and One-pot RAFT Synthesis in Water. *Macromol. Rapid Commun.* **2011,** *32*, 1270-1276.

52. Chaduc, I.; Girod, M.; Antoine, R.; Charleux, B.; D'Agosto, F.; Lansalot, M., Batch Emulsion Polymerization Mediated by Poly(methacrylic acid) MacroRAFT Agents: One-Pot Synthesis of Self-Stabilized Particles. *Macromolecules* **2012,** *45*, 5881-5893.

53. Poon, C. K.; Tang, O.; Chen, X.-M.; Pham, B. T. T.; Gody, G.; Pollock, C. A.; Hawkett, B. S.; Perrier, S., Preparation of Inert Polystyrene Latex Particles as MicroRNA Delivery Vectors by Surfactant-Free RAFT Emulsion Polymerization. *Biomacromolecules* **2016,** *17*, 965-973.

54. Zetterlund, P. B.; Thickett, S. C.; Perrier, S.; Bourgeat-Lami, E.; Lansalot, M., Controlled/Living Radical Polymerization in Dispersed Systems: An Update. *Chem. Rev.* **2015,** *115*, 9745-9800.

55. Mable, C. J.; Warren, N. J.; Thompson, K. L.; Mykhaylyk, O. O.; Armes, S. P., Framboidal ABC triblock copolymer vesicles: a new class of efficient Pickering emulsifier. *Chem. Sci.* **2015,** *6*, 6179-6188.

56. Tan, J.; Sun, H.; Yu, M.; Sumerlin, B. S.; Zhang, L., Photo-PISA: Shedding Light on Polymerization-Induced Self-Assembly. *ACS Macro Letters* **2015,** *4*, 1249-1253.

57. Li, M.; De, P.; Gondi, S. R.; Sumerlin, B. S., End group transformations of RAFT-generated polymers with bismaleimides: Functional telechelics and modular block copolymers. *J. Polym. Sci., Part A: Polym. Chem.* **2008,** *46*, 5093-5100.

58. Perrier, S.; Takolpuckdee, P., Macromolecular design via reversible addition–fragmentation chain transfer (RAFT)/xanthates (MADIX) polymerization. *J. Polym. Sci., Part A: Polym. Chem.* **2005,** *43*, 5347-5393.

59. Lovett, J. R.; Warren, N. J.; Ratcliffe, L. P. D.; Kocik, M. K.; Armes, S. P., pH-Responsive Non-Ionic Diblock Copolymers: Ionization of Carboxylic Acid End-Groups Induces an Order–Order Morphological Transition. *Angew. Chem. Int. Ed.* **2015,** *54*, 1279-1283.

60. Lovett, J. R.; Warren, N. J.; Armes, S. P.; Smallridge, M. J.; Cracknell, R. B., Order–Order Morphological Transitions for Dual Stimulus Responsive Diblock Copolymer Vesicles. *Macromolecules* **2016,** *49*, 1016-1025.

61. Penfold, N. J. W.; Lovett, J. R.; Warren, N. J.; Verstraete, P.; Smets, J.; Armes, S. P., pH-Responsive non-ionic diblock copolymers: protonation of a morpholine end-group induces an order–order transition. *Polym. Chem.* **2016,** *7*, 79-88.

62. Penfold, N. J. W.; Lovett, J. R.; Verstraete, P.; Smets, J.; Armes, S. P., Stimulus-responsive non-ionic diblock copolymers: protonation of a tertiary amine end-group induces vesicle-to-worm or vesicle-to-sphere transitions. *Polym. Chem.* **2017,** *8*, 272-282.

63. Gibson, R. R.; Armes, S. P.; Musa, O. M.; Fernyhough, A., End-group ionisation enables the use of poly(N-(2-methacryloyloxy)ethyl pyrrolidone) as an electrosteric stabiliser block for polymerisation-induced self-assembly in aqueous media. *Polym. Chem.* **2019,** *10*, 1312-1323.

64. Beltramo, P. J.; Gupta, M.; Alicke, A.; Liascukiene, I.; Gunes, D. Z.; Baroud, C. N.; Vermant, J., Arresting dissolution by interfacial rheology design. *Proceedings of the National Academy of Sciences* **2017,** *114*, 10373-10378.

65. Golemanov, K.; Tcholakova, S.; Kralchevsky, P. A.; Ananthapadmanabhan, K. P.; Lips, A., Latex-Particle-Stabilized Emulsions of Anti-Bancroft Type. *Langmuir* **2006,** *22*, 4968-4977.

66. Tcholakova, S.; Denkov, N. D.; Lips, A., Comparison of solid particles, globular proteins and surfactants as emulsifiers. *Phys. Chem. Chem. Phys.* **2008,** *10*, 1608-1627.

67. Wang, H.; Singh, V.; Behrens, S. H., Image Charge Effects on the Formation of Pickering Emulsions. *The Journal of Physical Chemistry Letters* **2012,** *3*, 2986-2990.

68. Tambe, D. E.; Sharma, M. M., Factors Controlling the Stability of Colloid-Stabilized Emulsions: I. An Experimental Investigation. *J. Colloid Interface Sci.* **1993,** *157*, 244-253.

69. Ridel, L.; Bolzinger, M.-A.; Gilon-Delepine, N.; Dugas, P.-Y.; Chevalier, Y., Pickering emulsions stabilized by charged nanoparticles. *Soft Matter* **2016,** *12*, 7564-7576.

70. Marinova, K. G.; Alargova, R. G.; Denkov, N. D.; Velev, O. D.; Petsev, D. N.; Ivanov, I. B.; Borwankar, R. P., Charging of Oil−Water Interfaces Due to Spontaneous Adsorption of Hydroxyl Ions. *Langmuir* **1996,** *12*, 2045-2051.

71. Roger, K.; Cabane, B., Why Are Hydrophobic/Water Interfaces Negatively Charged? *Angew. Chem. Int. Ed.* **2012,** *51*, 5625-5628.

72. Binks, B. P.; Whitby, C. P., Nanoparticle silica-stabilised oil-in-water emulsions: improving emulsion stability. *Colloids Surf., A* **2005,** *253*, 105-115.

73. Reincke, F.; Hickey, S. G.; Kegel, W. K.; Vanmaekelbergh, D., Spontaneous Assembly of a Monolayer of Charged Gold Nanocrystals at the Water/Oil Interface. *Angew. Chem. Int. Ed.* **2004,** *43*, 458-462.

74. Ilavsky, J.; Jemian, P. R., Irena: tool suite for modeling and analysis of small-angle scattering. *J. Appl. Crystallogr.* **2009,** *42*, 347-353.

75. Walter, J.; Thajudeen, T.; Su, S.; Segets, D.; Peukert, W., New possibilities of accurate particle characterisation by applying direct boundary models to analytical centrifugation. *Nanoscale* **2015,** *7*, 6574-6587.

76. Larson-Smith, K.; Jackson, A.; Pozzo, D. C., SANS and SAXS Analysis of Charged Nanoparticle Adsorption at Oil–Water Interfaces. *Langmuir* **2012,** *28*, 2493-2501.

77. Balmer, J. A.; Mykhaylyk, O. O.; Schmid, A.; Armes, S. P.; Fairclough, J. P. A.; Ryan, A. J., Characterization of Polymer-Silica Nanocomposite Particles with Core–Shell Morphologies using Monte Carlo Simulations and Small Angle X-ray Scattering. *Langmuir* **2011,** *27*, 8075-8089.

78. Roe, R.-J., *Methods of X-ray and Neutron Scattering in Polymer Science*. Oxford University Press: New York, 2000.

79. Juárez, J. A.; Whitby, C. P., Oil-in-water Pickering emulsion destabilisation at low particle concentrations. *J. Colloid Interface Sci.* **2012,** *368*, 319-325.

80. Pawar, A. B.; Caggioni, M.; Ergun, R.; Hartel, R. W.; Spicer, P. T., Arrested coalescence in Pickering emulsions. *Soft Matter* **2011,** *7*, 7710-7716.

81. Fouilloux, S.; Malloggi, F.; Daillant, J.; Thill, A., Aging mechanism in model Pickering emulsion. *Soft Matter* **2016,** *12*, 900-904.

82. Nazarzadeh, E.; Anthonypillai, T.; Sajjadi, S., On the growth mechanisms of nanoemulsions. *J. Colloid Interface Sci.* **2013,** *397*, 154-162.

83. Schmitt, V.; Cattelet, C.; Leal-Calderon, F., Coarsening of Alkane-in-Water Emulsions Stabilized by Nonionic Poly(oxyethylene) Surfactants: The Role of Molecular Permeation and Coalescence. *Langmuir* **2004,** *20*, 46-52.

84. Mun, S.; McClements, D. J., Influence of Interfacial Characteristics on Ostwald Ripening in Hydrocarbon Oil-in-Water Emulsions. *Langmuir* **2006,** *22*, 1551-1554.